Do Chemical Reactions React along the Reaction Path?

B. Hartke and J. Manz*

Contribution from the Institut für Physikalische Chemie, Universität Würzburg, Marcusstrasse 9-11, D-8700 Würzburg, Germany. *Received October 13, 1987*

Abstract: In contrast with traditional intuition, chemical reactions may proceed far away from reaction paths (defined as paths of steepest descents starting at the systems' potential barriers). This is demonstrated and explained by classical trajectory simulations and quantum vibrationally near-adiabatic hyperspherical representations of an exoergic collinear hydrogen-transfer reaction with two isotopic variants, F + DBr(v) → FD + Br and F + MuBr(v) → FMu + Br, with energies well above the classical reaction thresholds. The reactants leave the reaction path by vibrationally induced light atom transfer at large distances between the heavy atoms, i.e. by cutting the corner between the educt and product valleys of the potential energy surface (without tunneling). These shortcuts are particularly prominent if the reaction path penetrates into the dynamical white spot covering the potential corner. Strong detours away from the reaction path may be induced by vibrational excitation (v) of educts or by decreasing the mass of the transferred atom. Detours by tunneling are complementary to vibrationally induced corner cutting. The model systems demonstrate the important and possibly dominant role of reaction dynamics in comparison with static properties of the reaction path.

1. Introduction

Chemical intuition and tradition assume that chemical reactions react along a minimum energy path, the reaction path ξ.[1] This view is summarized by the familiar textbook diagram showing the system's potential energy surface V versus ξ, usually from educts via the potential barrier ‡ to products. Of course, this is just a simplified representation of ξ, which may be defined as path of steepest descent from the potential barrier(s) ‡ toward the educt and product valleys of V, imbedded in multidimensional space of the system's internal coordinates (for recent reviews see ref 2 and 3). Thus ξ is defined as the minimum potential energy path depending exclusively on static properties of the potential V, irrespective of the system's reaction dynamics. Nevertheless, the static properties of ξ and its surroundings, including locations and heights of potential barriers ‡, curvature, and vibrational frequencies of normal modes orthogonal to ξ, are often related to chemical reaction dynamics, rate coefficients, or product distributions.[1,3-5] However, without bias, such relations are by no means trivial.

Do chemical reactions really react along ξ? Of course, one important exception is well-known: At low temperatures or energies, in particular below the classical reaction threshold, the educts will avoid climbing the barrier ‡ by tunneling, and the preferential tunneling paths,[1d,6,7] e.g. Marcus–Coltrin paths[8] or least action (ground-state) tunneling paths,[9] may deviate from curved reaction paths, cutting the corner on their convex sides; for reviews see ref 3, 6c, and 10.

To the best of our knowledge, similar systematic deviations from ξ have not been reported previously for highly excited educts, although this observation might be conjectured by extrapolation of the low-energy tunneling results. Of course, individual classical trajectories simulating the chemical reaction hardly ever coincide with ξ. Nevertheless, traditional chemical intuition states that typical trajectories propagate close to ξ, so that representative ensembles of trajectories or corresponding quantum wave packets should follow and cover ξ. Accordingly, a comparative study of HFH, H_3 and ClH_2 resonances did not yield any outstanding preference of decays along "dynamical reaction paths" different from minimum energy reaction paths.[11] However, a rather exceptional analysis of quantum fluxes for the collinear reaction H + $H_2(v = 0)$ → $H_2(v' = 0)$ + H indicates stimulating tunneling deviations even slightly above the classical threshold, together with the intriguing development of regions of dynamic inaccessibility as the initial relative kinetic energy increases.[7]

In this paper, we present novel strong and systematic detours away from ξ in special cases of exoergic elementary hydrogen-transfer reactions. As a model system we consider two isotopic variants of the collinear reaction shown in eq 1.1 with vibrational

$$F + HBr(v) \rightarrow FH + Br \qquad (1.1)$$

(1) (a) Eyring, H.; Polanyi, M. *Z. Phys. Chem., Abt. B* **1931**, *B12*, 279. (b) Glasstone, S.; Laidler, K. J.; Eyring, H. *The Theory of Rate Processes*; McGraw-Hill: New York, 1941. (c) Hofacker, G. L. *Z. Naturforsch., A: Astrophys., Phys. Phys. Chem.* **1963**, *A18*, 607. (d) Marcus, R. A. *J. Chem. Phys.* **1966**, *45*, 4493, 4500; **1968**, *49*, 2610, 2617. (e) Fukui, K. *J. Phys. Chem.* **1970**, *74*, 4161. *Acc. Chem. Res.* **1981**, *14*, 363. (f) Fukui, K.; Kato, S.; Fujimoto, H. *J. Am. Chem. Soc.* **1975**, *97*, 1. (g) Chapuisat, X.; Nauts, A.; Durand, G. *Chem. Phys.* **1981**, *56*, 91. (h) Laidler, K.; King, M. C. *J. Phys. Chem.* **1983**, *87*, 2657.

(2) (a) Müller, K. *Angew. Chem.* **1980**, *92*, 1. (b) Truhlar, D. G.; Brown, F. B.; Steckler, R.; Isaacson, A. D. In *The Theory of Chemical Reaction Dynamics*; Clary, D. C., Ed.; Reidel: Dordrecht, The Netherlands, 1986; p 285. (c) Truhlar, D. G.; Steckler, R.; Gordon, M. S. *Chem. Rev.* **1987**, *87*, 217.

(3) Truhlar, D. G.; Isaacson, A. D.; Garrett, B. C. In *Theory of Chemical Reaction Dynamics*; Baer, M., Ed.; Chemical Rubber Co.: Boca Raton, FL, 1985; Vol. IV, p 65.

(4) (a) Miller, W. H. *J. Chem. Phys.* **1974**, *61*, 1823. (b) Miller, W. H.; Handy, N. C.; Adams, J. E. *J. Chem. Phys.* **1980**, *72*, 99. (c) Miller, W. H. In *Potential Energy Surfaces and Dynamics Calculations*; Truhlar, D. G., Ed.; Plenum: New York, 1981; p 265. (d) Gray, S. K.; Miller, W. H.; Yamaguchi, Y.; Schaefer, H. F. *J. Am. Chem. Soc.* **1981**, *103*, 1900. (e) Waite, B. A.; Gray, S. K.; Miller, W. H. *J. Chem. Phys.* **1983**, *78*, 259. (f) Miller, W. H. *J. Am. Chem. Soc.* **1983**, *105*, 216. (g) Miller, W. H.; Schwartz, S. D.; Tromp, J. W. *J. Chem. Phys.* **1983**, *79*, 4889. (h) Miller, W. H. *J. Chem. Phys.* **1984**, *81*, 3573. (i) Carrington, T., Jr.; Miller, W. H. *J. Chem. Phys.* **1986**, *84*, 4364. (j) Miller, W. H. In *The Theory of Chemical Reaction Dynamics*; Clary, D. C., Ed.; Reidel: Dordrecht, The Netherlands, 1986; p 27.

(5) (a) Hofacker, G. L.; Levine, R. D. *Chem. Phys. Lett.* **1971**, *9*, 617. (b) Russegger, P.; Brickmann, J. *J. Chem. Phys.* **1975**, *62*, 1086; **1977**, *66*, 1. (c) Ishida, K.; Morokuma, K.; Komornicki, A. *J. Chem. Phys.* **1977**, *66*, 2153. (d) Kato, S.; Kato, H.; Fukui, K. *J. Am. Chem. Soc.* **1977**, *99*, 684.

(6) (a) Truhlar, D. G.; Kuppermann, A. *J. Chem. Phys.* **1972**, *56*, 2232. (b) Kuppermann, A. *Theor. Chem. (N.Y.)* **1981**, *6A*, 79. (c) Schatz, G. C. *Chem. Rev.* **1987**, *87*, 81. (d) Tachibana, A.; Fueno, H.; Yamabe, T. *J. Am. Chem. Soc.* **1986**, *108*, 4346.

(7) Kuppermann, A.; Adams, J. T.; Truhlar, D. G. In *Abstracts of Papers of the 8th International Conference on the Physics of Electronic and Atomic Collisions*; Cobić, B. C., Kurepa, M. V., Eds.; Institute of Physics: Beograd, 1973; p 149.

(8) (a) Marcus, R. A.; Coltrin, M. *J. Chem. Phys.* **1977**, *67*, 2609. (b) Garrett, B. C.; Truhlar, D. G. *J. Phys. Chem.* **1979**, *83*, 200, 1079, 3058(E); **1980**, *84*, 682(E); **1983**, *87*, 4553(E). (c) Altkorn, R. I.; Schatz, G. C. *J. Chem. Phys.* **1980**, *72*, 3337.

(9) (a) Miller, W. H.; George, T. F. *J. Chem. Phys.* **1972**, *56*, 5668. (b) Garrett, B. C.; Truhlar, D. G.; Wagner, A. F.; Dunning, T. H., Jr. *J. Chem. Phys.* **1983**, *78*, 4400. (c) Bondi, D. K.; Connor, J. N. L.; Garrett, B. C.; Truhlar, D. G. *J. Chem. Phys.* **1983**, *78*, 5981. (d) Garrett, B. C.; Truhlar, D. G. *J. Chem. Phys.* **1983**, *79*, 4931. (e) Garrett, B. C.; Abusalbi, N.; Kouri, D. J.; Truhlar, D. G. *J. Chem. Phys.* **1985**, *83*, 2252. (f) Kreevoy, M. M.; Ostović, D.; Truhlar, D. G.; Garrett, B. C. *J. Phys. Chem.* **1986**, *90*, 3766. (g) Garrett, B. C.; Truhlar, D. G.; Schatz, G. C. *J. Am. Chem. Soc.* **1986**, *108*, 2876. (h) Clary, D. C. *J. Chem. Phys.* **1985**, *83*, 1685.

(10) Truhlar, D. G.; Garrett, B. C. *J. Chim. Phys. Phys.-Chim. Biol.* **1987**, *84*, 365.

(11) Garrett, B. C.; Truhlar, D. G. *J. Phys. Chem.* **1982**, *86*, 1136.

0002-7863/88/1510-3063$01.50/0

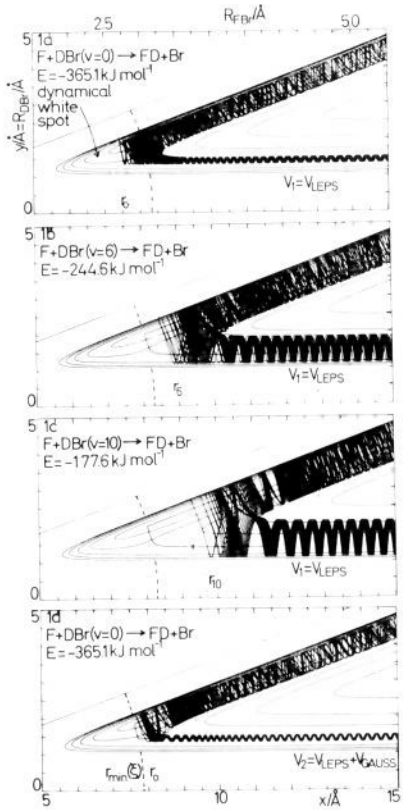

Figure 1. Classical trajectory simulation of the collinear F + DBr(v) → FD + Br reaction with total energy $E_{total} = E = E_v + E_{trans}$ and collision energy E_{trans} = 2 kJ mol^{-1}. Equipotential contours $V_{1,2}(x, y) = -100$, -200, ..., -500 kJ mol^{-1} are presented with mass-weighted coordinates $x \approx 2.8R_{FBr}$ and $y = R_{DBr}$. The angle ϕ_m between educt and product valleys is marked by the abscissa and the straight ascending line. The reaction path ξ passes via the potential barrier ‡. The radial limits $r_{min}(\xi)$ of ξ are indicated by dashed lines. The radial limits r_v of the classical trajectories are indicated by dotted lines. They also mark the boundary of the dynamical white spot, together with the equipotential contour $V(x, y) = E_{total}$ which may be extrapolated approximately from the envelope of the trajectories.

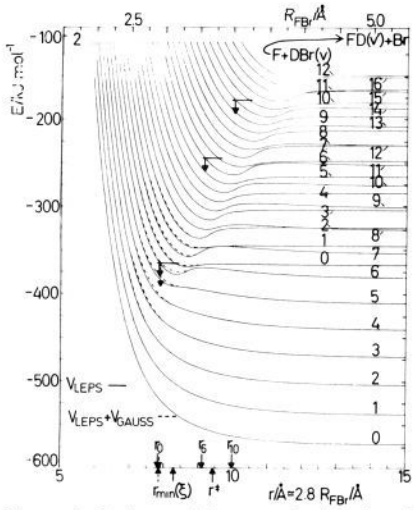

Figure 2. Hyperspherical potential curves $\mathcal{E}_{v_3}$ for the collinear F + DBr(v) → FD(v') + Br reaction versus hyperspherical radius $r \approx 2.8R_{FBr}$. Asymptotically, the $\mathcal{E}_{v_3}(r)$ correlate with educt F + DBr(v) and product FD(v') + Br levels E_v and $E_{v'}$ as indicated by quantum numbers v and v'. Continuous and dashed lines correspond to potentials $V_1 = V_{LEPS}$ and $V_2 = V_{LEPS} + V_{Gauss}$, respectively. The total energies E of reactions F + DBr(v = 0, 6, and 10) at E_{trans} = 2 kJ mol^{-1} collision energies are indicated by horizontal bars. The vertical arrows mark the resulting approximate turning points r_v for quantum wave packets simulating the reactions. These quantum $r_{v,qu}$ correspond to the classical $r_{v,cl}$ determined in parts a–d of Figure 1. For comparison, the radial boundary $r_{min}(\xi)$ of the reaction path and the location of the saddle point $r^‡$ are also given.

educt stats v, at energies well above the tunneling regime. This system is a favorable candidate, since it exhibits several strong dynamical effects, including population inversion of products, approximate conservation of translational energy, and oscillatory reactivity,[12-16] which turn out to be important.

The present search for novel deviations of reaction 1.1 from its intrinsic reaction path ξ has been motivated by the recent discovery of a "dynamical white spot" on the potential energy surface of reaction 1.1,[15] which in turn is a consequence of a dynamical effect discovered by J. C. Polanyi et al.,[17] i.e. vibrationally induced corner cutting, as follows: For light-atom-transfer systems such as reaction 1.1 and for energies above the classical threshold, the central vibrating atom may hop from one heavy atom to the other at rather long distances (without tunneling). In corresponding classical simulations, real trajectories switch from the educt to the product valleys of the potential energy surface, cutting the corner between these valleys. This corner is energetically accessible (in contrast with the case of tunneling where it is inaccessible) but dynamically off-limits: It constitutes a dynamical white spot, never visited by any classical trajectories or corresponding quantum wave packets. In consequence, hydrogen-transfer reactions should leave the reaction path if ξ penetrates into the dynamical white spot!

It is important to distinguish Polanyi and co-workers' vibrationally induced corner cutting[17] from tunneling-induced corner cutting.[3,6-10] The first mechanism, which is fundamental for the present paper, requires energies above the classical threshold; the second may occur at lower energies. The first may be described with real classical trajectories; the second requires complex ones. The first is due to exclusive dynamic constraints, and the second, to energetic ones. Nevertheless, both mechanisms yield the same net effect: corner cutting. This similarity also suggests that vibrationally induced corner cutting at high energies might cause detours from ξ, similar to tunneling-induced corner cutting, but independently and with possibly different energetic trends.

In the following, we shall test this working hypothesis and search for situations where the reaction path is covered, in part, by the dynamical white spot. For this purpose we extend our previous investigation[15] to more extreme situations of (i) high-vibrational excitation of educts, (ii) isotopic substitution, and (iii) reaction dynamics on modified potential energy surfaces.

2. Models and Techniques

For subsequent investigations of isotope effects, we consider two variants of the collinear hydrogen-transfer reaction 1.1, i.e. eq 2.1 and 2.2, where the hydrogen atom is replaced by deuterium or muonium. The

$$F + DBr(v) \rightarrow FD + Br \quad (2.1)$$

$$F + MuBr(v) \rightarrow FMu + Br \quad (2.2)$$

masses used are m_{Mu} = 0.11397, m_D = 2.014, m_F = 19.00, and m_{Br} = 79.91 amu. Muonium-transfer reactions have been studied previously in ref 9c,d, 18, and 19.

(12) Jonathan, N. B. H.; Sellers, P. V.; Stace, A. J. *Mol. Phys.* **1981**, *43*, 215.
(13) (a) Würzberg, E.; Houston, P. L. *J. Chem. Phys.* **1980**, *72*, 5915. (b) Tamagake, K.; Setser, D. W.; Sung, J. P. *J. Chem. Phys.* **1980**, *73*, 2203. (c) Smith, I. W. M.; Wrigley, D. J. *Chem. Phys.* **1981**, *63*, 321. (d) Dill, B.; Heydtmann, H. *Chem. Phys.* **1983**, *81*, 419. (e) Dzelzkalns, L. S.; Kaufman, F. *J. Chem. Phys.* **1983**, *79*, 3836. (f) Aker, P. M.; Donaldson, D. J.; Sloan, J. J. *J. Phys. Chem.* **1986**, *90*, 3110.
(14) (a) Manz, J.; Schor, H. H. R. *Chem. Phys. Lett.* **1984**, *107*, 549. (b) Gertitschke, P. L.; Manz, J.; Römelt, J.; Schor, H. H. R. *J. Chem. Phys.* **1985**, *83*, 208. (c) Coveney, P. V.; Child, M. S.; Römelt, J. *Chem. Phys. Lett.* **1985**, *120*, 349.
(15) (a) Gertitschke, P. L.; Kiprof, P.; Manz, J. *J. Chem. Phys.* **1987**, *87*, 941. (b) Gertitschke, P. L. Diplomarbeit, Technische Universität München, 1986. (c) Bisseling, R. H.; Gertitschke, P. L.; Kosloff, R.; Manz, J. *J. Chem. Phys.*, in press.
(16) (a) Manz, J. *Comments At. Mol. Phys.* **1985**, *17*, 91. (b) Römelt, J. In *The Theory of Chemical Reaction Dynamics*; Clary, D. C., Ed.; Reidel: Dordrecht, The Netherlands, 1986; p 77. (c) Manz, J. In *Molecules in Physics, Chemistry and Biology*; Maruani, J., Ed.; Reidel: Dordrecht, The Netherlands, 1987; Vol. 3.
(17) (a) Parr, C. A.; Polanyi, J. C.; Wong, W. H. *J. Chem. Phys.* **1973**, *58*, 5. (b) Polanyi, J. C.; Schreiber, J. L. In *Physical Chemistry, An Advanced Treatise, Kinetics of Gas Reactions*; Jost, W., Ed.; Academic: New York, 1974; Vol. 6A, p 383.

The reactions are described in terms of mass-weighted coordinates (eq 2.3a and 2.3b) for X = D and Mu. Here $m_{F,XBr}$ and $m = m_{XBr}$ are the reduced masses of the F + XBr and XBr systems, R_{XBr} is the XBr bond length, and $R_{F,XBr}$ is the distance from F to the center of mass of XBr.

$$x = (m_{F,XBr}/m)^{1/2} R_{F,XBr} = r \cos \phi \tag{2.3a}$$

$$y = R_{XBr} = r \sin \phi \tag{2.3b}$$

Equation 2.3 also defines the hyperspherical radius r and polar angle ϕ, as adapted e.g. from ref 14, 15, and 19; for reviews see ref 16. The ranges of r and ϕ are shown in eq 2.4a and 2.4b with skew angle given in eq 2.5. The light mass of the transferred atom, X = Mu or D,

$$0 < r < \infty \tag{2.4a}$$

$$0 < \phi < \phi_m \tag{2.4b}$$

$$\phi_m = \arctan\,[m_X(m_F + m_X + m_{Br})/m_F m_{Br}]^{1/2} \tag{2.5}$$

between its heavy partners F and Br implies that ϕ_m is rather small (eq 2.5a and 2.5b see Figures 1 and 3). As a consequence, the mass-

$$\phi_m = 20.1° \text{ for F + DBr} \tag{2.5a}$$

$$\phi_m = 4.9° \text{ for F + MuBr} \tag{2.5b}$$

weighted coordinate x as well as the hyperspherical radius r is approximately proportional to the distances between the heavy atoms (eq 2.6a and 2.6b). Therefore, educt and product translations are essentially

$$r \approx x \approx 2.8 R_{FBr} \text{ for F + DBr} \tag{2.6a}$$

$$r \approx x \approx 11.6 R_{FBr} \text{ for F + MuBr} \tag{2.6b}$$

along r, whereas vibrations of the central atom X between F and Br are along ϕ, ranging from $\phi \to 0$ for the F + XBr configuration to $\phi \to \phi_m$ for FX + Br.

The FXBr interactions are modeled with two potential energy surfaces V. The first one (eq 2.7) is the best extended LEPS potential of Jonathan et al.,[12] with the parameters presented in Table 3 of ref 12. This po-

$$V_1 = V_{LEPS} \tag{2.7}$$

tential has already been used in several studies of the F + HBr reaction.[12,14-16] The second potential (eq 2.8) is a modified LEPS potential

$$V_2 = V_{LEPS} + V_{Gauss} \tag{2.8}$$

with a small Gaussian shoulder superimposed on the LEPS potential *ridge* separating the educt and product potential valleys. It is applied exclusively to the FDBr system below. Similar modified LEPS potentials have been used previously, e.g. for model simulations of the H + F_2 *reaction*[20] *or hydride transfers among nitrogen heterocycles.*[9f]

Contour plots of $V_1(x, y)$ and $V_2(x, y)$ are shown in parts a–c and d of Figure 1, respectively. They are hardly distinguishable; in fact, the differences between V_1 and V_2 are possibly even smaller than deviations between V_1 or V_2 and the exact F + XBr potential, which is unknown. Explicitly,

$$V_2 - V_1 = V_{Gauss} = A \exp[-[f_1(x - c_1)^2 + f_2(x - c_1)(y - c_2) + f_3(y - c_2)^2]] \tag{2.9}$$

with $f_1 = (\cos^2 \alpha)/a^2 + (\sin^2 \alpha)/b^2$, $f_2 = 2 \sin \alpha \cos \alpha\,(1/a^2 - 1/b^2)$, and $f_3 = (\sin^2 \alpha)/a^2 + (\cos^2 \alpha)/b^2$ and parameters $c_1 = 7.75$ Å, $c_2 = 1.475$ Å, $\alpha = 5.71°$, $A = 12.0$ kJ mol^{-1}, $a = 1.25$ Å, and $b = 0.05$ Å (1 Å = 10^{-10} m).

One relevant consequence of the Gaussian modification (eq 2.9) is that the reaction path ξ_2 of V_2 is shifted farther into the potential corner than ξ_1 of V_1. Quantitatively, the closest approach of ξ to the three-atom coincidence is

$$r_{min}(\xi_1) = 8.3 \text{ Å for } V_1 \qquad r_{min}(\xi_2) = 7.8 \text{ Å for } V_2 \tag{2.10}$$

Other relevant properties of V_1 and V_2 are listed in Table I. This comparison demonstrates the similarity of model potentials V_1 and V_2.

Table I. Barrier Properties of F + DBr Model Potential Energy Surfaces[a]

	$V_1 = V_{LEPS}$[b]	$V_2 = V_{LEPS} + V_{Gauss}$[c]		$V_1 = V_{LEPS}$[b]	$V_2 = V_{LEPS} + V_{Gauss}$[c]
ΔV	1.639	1.639	$y = R_{DBr}$	1.419	1.420
R_{FBr}	3.362	3.362	x	9.322	9.323
R_{FD}	1.942	1.943	r	9.430	9.430

[a] Barrier heights in kilojoules per mole; distances in angstroms. R_{AB} = distance from A to B; x, y = mass-weighted cartesian coordinates; r = hyperspherical radius (eq 2.3). [b] Reference 12; Table III. [c] Equations 2.8 and 2.9.

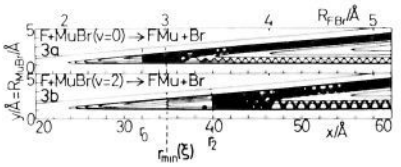

Figure 3. Classical trajectory simulations of the collinear F + MuBr(v) → FMu + Br reaction with total energy $E_{total} = E_v + E_{trans}$ and collision energy $E_{trans} = 20$ kJ mol^{-1} on the potential $V_1 = V_{LEPS}$ (notations as in Figure 1).

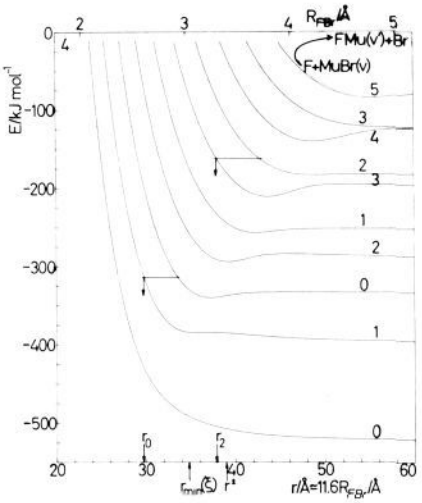

Figure 4. Hyperspherical potential curves $\epsilon_{v3}(r)$ for the collinear F + MuBr(v) → FMu(v') + Br reaction on potential $V_1 = V_{LEPS}$ (notations as in Figure 2). The quantum radial boundaries $r_{v,qu}$ for the F + MuBr(v = 0,2) reaction correspond to the classical $r_{v,cl}$ determined in parts a and b of Figure 3.

The reaction paths ξ are evaluated as usual[2] by propagating the potential gradients from the barriers ‡ toward the educt and product valleys. The gradients $\nabla V = (\partial V/\partial x, \partial V/\partial y)$ are calculated by numerically converged finite differences, with small step-size $\Delta\xi = 0.001$ Å.

Classical trajectory simulations are carried out as explained in detail in ref 15a (see also ref 21). In particular, representative ensembles of typically 25–500 trajectories equidistant in phase are generated in the educt potential valley. Many of them turn out to be nonreactive, due to the small F + DBr and F + MuBr reaction propabilities[14-16] at small collision energies. The reactive trajectories are plotted in Figure 1, starting out from the educt valley as oscillatory ribbon, which unravels in the interaction region before leaking out into the product valley. The initial ribbons indicate F + XBr reactivity bands.[15,22] The numbers of representative trajectories shown in Figure 1, typically 12, are sufficient for the subsequent conclusions.

The classical trajectories correspond to quantum wave packets Ψ simulating reactions 2.1 and 2.2. In close analogy, $\Psi(t)$ may also be propagated from educts to products, i.e. by solving the time-dependent

(18) (a) Walker, D. C. *Muon and Muonium Chemistry*; Cambridge University: Cambridge, MA, 1983. (b) Roduner, E. *Prog. React. Kinet.* **1986**, *14*, 1.

(19) (a) Manz, J.; Römelt, J. *Chem. Phys. Lett.* **1980**, *76*, 337; **1981**, *81*, 179. (b) Manz, J.; Pollak, E.; Römelt, J. *Chem. Phys. Lett.* **1982**, *86*, 26. (c) Aquilanti, V.; Cavalli, S.; Laganà, A. *Chem. Phys. Lett.* **1982**, *93*, 179. (d) Hiller, C.; Manz, J.; Miller, W. H.; Römelt, J. *J. Chem. Phys.* **1983**, *78*, 3850. (e) Römelt, J. *Chem. Phys.* **1983**, *79*, 197. (f) Clary, D. C.; Connor, J. N. L. *J. Phys. Chem.* **1984**, *88*, 2758. (g) Bondi, D. K.; Connor, J. N. L.; Manz, J.; Römelt, J. *Mol. Phys.* **1983**, *50*, 467.

(20) Jakubetz, W. *Chem. Phys.* **1978**, *35*, 141.

(21) Truhlar, D. G.; Muckermann, J. T. In *Atom-Molecule Collision Theory: A Guide to the Experimentalist*; Bernstein, R. B., Ed.; Plenum: New York, 1979; p 505.

(22) Wright, J. S.; Tan, K. G. *J. Chem. Phys.* **1977**, *66*, 104.

Table II. Dynamics of Collinear F + XBr Reactions

reaction	energies[a]/kJ mol^{-1}		potential[b]	radial boundaries[c]/Å			reaction[d] along ξ	figures
	E_{trans}	E_{total}		$r_{min}(\xi)$	$r_{v,cl}$	$r_{v,qu}$		
F + DBr(v = 0) → FD + Br	2.0	−365.1	V_1	8.3	7.6	7.9	yes	1a,2
F + DBr(v = 6) → FD + Br	2.0	−244.6	V_1	8.3	8.8	9.2	no	1b,2
F + DBr(v = 10) → FD + Br	2.0	−177.6	V_1	8.3	9.7	10.0	no	1c,2
F + DBr(v = 0) → FD + Br	2.0	−365.1	V_2	7.8	7.9	7.9	no	1d,2
F + MuBr(v = 0) → FMu + Br	20.0	−313.1	V_1	34.8	32.2	30.0	yes	3a,4
F + MuBr(v = 2) → FMu + Br	20.0	−161.4	V_1	34.8	40.0	38.1	no	3b,4

[a] $E_{total} = E_{trans} + E_v$ measured from three-atom dissociation threshold. [b] $V_1 = V_{LEPS}$ (eq 2.7), and $V_2 = V_{LEPS} + V_{Gauss}$ (eq 2.8). [c] $r_{min}(\xi)$ = static limit of reaction path ξ (eq 2.10); $r_{v,d}$ and $r_{v,qu}$ = classical and quantum boundaries of dynamical white spot; see eq 2.13. [d] "No" if $r_{min}(\xi) < r_v$; see criterion 2.15.

Schrödinger equation numerically, with either mass-weighted cartesian or hyperspherical coordinates (eq 2.3), as in ref 15c and 23. A series of snapshots of $\Psi(x, y, t) \equiv \Psi(r, \phi, t)$ would then show directly whether the F + XBr wavepackets follow and cover the reaction path or not. However, explicit evaluations of $\Psi(t)$ are expensive.[23] Therefore, we use the more economic quantum vibrationally near-adiabatic hyperspherical representations of reactions 2.1 and 2.2, which allow us to compare the radial ranges of ξ and $\Psi(t)$ directly. This is sufficient for the present purpose. The technique is based on previous evaluations of reaction 2.1,[14-16] as follows.

The rather slow translational motion of heavy atoms F and Br in comparison with fast vibrations of X = Mu or D suggests a near-adiabatic, Born–Oppenheimer-type separation of motions along r and ϕ.[16,19,24] At fixed r, the angular Schrödinger equation is eq 2.11, yielding adiabatic

$$\left[\frac{-\hbar^2}{2mr^2}\frac{d^2}{d\phi^2} + V(\phi, r)\right]\Phi_{v_3}(\phi; r) = \mathcal{E}_{v_3}(r)\,\Phi(\phi; r) \qquad (2.11)$$

hyperspherical potential curves $\mathcal{E}_{v_3}(r)$ for the radial motion. These potential curves, adapted from ref 14–16 and extended to large hyperspherical vibrational quantum numbers v_3 for potentials V_1 and V_2, are shown in Figures 2 and 4 for the F + DBr and F + MuBr reactions, respectively. Asymptotically for $r \to \infty$, they approach the educt or product levels E_v or $E_{v'}$.

When eq 2.11 is used, reactions 2.1 and 2.2 may be represented by radial wave packets moving on the potential curves $\mathcal{E}_{v_3}(r)$ from educts F + XBr(v) at large r toward interaction configurations FXBr at small r and back to educts or to products FX(v') + Br at large r. During these radial translations, the orthogonal vibrations turn out to be nearly adiabatic, conserving their quantum number v_3; i.e., most collisions are elastic, and the small fraction of reactive collisions prefer transitions between neighboring hyperspherical potential curves, $v_3 \to v'_3 = v_3 \pm 1$. The reaction from F + XBr(v) to FX(v') + Br thus corresponds to radial motions along $\mathcal{E}_{v_3}(r)$ and $\mathcal{E}_{v_3\pm1}(r)$ with near-adiabatic transitions between these potential curves. In the asymptotic limit

$$E_v = \mathcal{E}_{v_3}(r \to \infty) \approx \mathcal{E}_{v_3\pm1}(r \to \infty) = E_{v'} \qquad (2.12)$$

This result indicates approximate conservation of vibrational energy (measured from the three-atom dissociation threshold) or, equivalently, Baer's rule[25] (see also ref 14–16), i.e. approximate conservation of translational energy. Note that rule 2.12 implies strong population inversion of products; e.g., educts F + DBr(v = 0) yield primarily products FD(v' = 6) + Br.[14,15]

The near adiabaticity (eq 2.12) is supported by several previous studies not only for the F + XBr reactions[14-16] but equivalently for similar hydrogen-transfer reactions.[9e,19,24,26] For example, oscillatory quantum reaction probabilities are well reproduced by approximate quantum or semiclassical evaluations, which use exclusively two neighboring hyperspherical potential curves correlating with (near-) degenerate educt and product levels $E_v \approx E_{v'}$.[14c,19c,d,g,24]

As a consequence of the vibrational near adiabaticity (eq 2.12), the radial range of quantum wave packets simulating the reaction F + XBr(v) → FX(v') + Br coincides with the accessible range of the potential curve $\mathcal{E}_{v_3-1}(r)$, which includes the ranges of $\mathcal{E}_{v_3}$ and $\mathcal{E}_{v_3-1}$ (see Figures 2 and 4). Therefore, the radial range explored by educts F + DBr(v = 0) at total energy E_{total} is essentially from $r = \infty$ to the classical turning point r_v defined by eq 2.13. In principle, smaller values $r < r_v$

$$E_{total} = \mathcal{E}_{v_3-1}(r_v) \text{ for } \mathcal{E}_{v_3} = E_v \qquad (2.13)$$

may be reached by tunneling or diabatic transitions; however, these effects are negligible.[14-16] When eq 2.13 is used, the radial range covered by reactions 2.1 and 2.2 can be determined graphically with the plots of the potential curves $\mathcal{E}_{v_3}(r)$ (cf. Figures 2 and 4).

Quantum–classical correspondence suggests that the radial ranges of quantum wave packets and classical trajectories should be similar; i.e., the quantum limit $r_{v,qu}$ of eq 2.13 should agree approximately with the radial boundary $r_{v,cl}$ to classical trajectories simulating the F + XBr(v) reaction. Approximate values of $r_{v,cl}$ are determined with the representative ensemble of trajectories shown in Figures 1 and 3. Thus, we anticipate eq 2.14.

$$r_{v,qu} \approx r_{v,cl} \approx r_v \qquad (2.14)$$

By definition, r_v is the upper radial boundary of the dynamical white spot of the potential that is inaccessible to quantum wave packets or trajectories simulating the F + XBr reactions. This dynamical boundary r_v (eq 2.14) should now be compared with the static radial limit $r_{min}(\xi)$ (eq 2.10) of the reaction path. The criterion (eq 2.15) would indicate that ξ penetrates into the dynamical white spot; i.e., the reaction does not react along ξ.

$$r_{min}(\xi) < r_v \qquad (2.15)$$

3. Results

3.1. Vibrationally Induced Corner Cutting. Effects of vibrational excitation of educts are demonstrated exemplarily by a series of classical trajectory simulations of the F + DBr(v) reaction 2.1 on the LEPS potential V_1 (eq 2.7) for v = 0, 6, 10. The results are shown in parts a–c of Figure 1 and summarized in Table II, together with the collision energies and other relevant information. Obviously, ground-state educts follow the reaction path ξ, which is hardly visible in Figure 1a because it is covered by the representative ensemble of F + DBr(v = 0) trajectories. However, the situation changes dramatically upon vibrational excitation of educts: As v increases, the dynamical white spot spreads out and eventually starts to sweep the trajectories from the reaction path ξ (see Figure 1b,c). Quantitatively, the dynamical boundaries $r_{v,cl}$ to classical trajectories exceed the static radial limit $r_{min}(\xi)$ of the reaction path as soon as $v \geq 4$; i.e., educts F + DBr(v) leave the reaction path if $v \geq 4$.

The detours of the F + DBr($v \geq 4$) reaction from ξ may be interpreted as consequence of vibrationally induced corner cutting, a dynamical effect studied previously only for ground-state or moderately excited educts:[15,17] Larger vibrational energy E_v of educts implies larger vibrational amplitudes and momenta perpendicular to the reaction path ξ. Consequently, the trajectories are inclined to change valleys earlier; i.e., the hydrogen atom is transferred at larger distances between the heavy atoms.

The systematic increase of the classical boundaries $r_{v,cl}$ also corresponds to an equivalent increase of the quantum boundaries

(23) (a) McCullough, E. A.; Wyatt, R. E. *J. Chem. Phys.* **1971**, *54*, 3578. (b) Kosloff, R.; Kosloff, D. *J. Chem. Phys.* **1983**, *79*, 1823. (c) Bisseling, R. H.; Kosloff, R.; Manz, J. *J. Chem. Phys.* **1985**, *83*, 993. (d) Mohan, V.; Sathyamurthy, N. *Comput. Phys. Rep.*, in press.

(24) (a) Babamov, V. K.; Marcus, R. A. *J. Chem. Phys.* **1981**, *74*, 1790. (b) Babamov, V. K.; Lopez, V.; Marcus, R. A. *J. Chem. Phys.* **1983**, *78*, 5621; *Chem. Phys. Lett.* **1983**, *101*, 507; *J. Chem. Phys.* **1984**, *80*, 1812; **1984**, *81*, 4181(E). (c) Abusalbi, N.; Kouri, D. J.; Lopez, V.; Babamov, V. K.; Marcus, R. A. *Chem. Phys. Lett.* **1984**, *103*, 458. (d) Nakamura, H. *J. Phys. Chem.* **1984**, *88*, 4812.

(25) Baer, M. *J. Chem. Phys.* **1975**, *62*, 305.

(26) (a) Kaye, J. A.; Kuppermann, A. *Chem. Phys. Lett.* **1981**, *77*, 573; **1982**, *92*, 574. (b) Shoemaker, C. L., Abusalbi, N.; Kouri, D. J. *J. Phys. Chem.* **1983**, *87*, 5389.

$r_{v,qu}$ upon vibrational educt excitations v (see Table II). The quantum results may be understood as consequence of the nested structure of potential curves $\mathcal{E}_0(r) < \mathcal{E}_1(r) < \mathcal{E}_2(r) < \ldots$ (cf. eq 2.11 and Figure 2): The larger the v, the higher is the energy of $\mathcal{E}_{v_3}(r)$ correlating with educt level E_v and the larger is the radial turning point r_v where quantum wave packets representing educts F + DBr(v) are reflected essentially to products FD(v') + Br (cf. eq 2.13).

The good agreement of quantum boundaries $r_{v,qu}$ with the classical ones $r_{v,cl}$, as anticipated in eq 2.14 and documented in Table II, confirms the deviations of the F + DBr($v \geq 4$) reaction from the reaction path ξ according to criterion 2.15. Incidentially, the equivalence of the quantum vibrationally near-adiabatic hyperspherical and classical trajectory representations is also supported by the rule of approximate conservation of vibrational energy, which has been derived quantum mechanically in eq 2.12 and corresponds to the very large vibrational amplitudes of highly excited products FD(v') + Br, as simulated classically in parts a–c of Figure 1.

3.2. Isotope Effects. Isotope effects are deduced by comparing classical trajectory simulations of the F + DBr(v) reaction 2.1 (see parts a–c of Figure 1) and their muonium-transfer analogues (eq 2.2) (see parts a and b of Figure 3). As in section 3.1, the classical results are supported by corresponding quantum vibrationally near-adiabatic hyperspherical representations of the F + DBr(v) and F + MuBr(v) reactions; compare Figures 2 and 4 as well as the resulting radial boundaries $r_{v,qu}$ of the F + DBr(v) and F + MuBr(v) reactions listed in Table II.

Obviously, both reactions 2.1 and 2.2 follow the reaction path ξ if starting out from ground-state educts, whereas vibrationally excited educts induce systematic deviations from the reaction path, as explained in section 3.1. However, the detours are considerably stronger for F + MuBr(v) than for F + DBr(v): Even educts F + MuBr($v = 2$) excited only to the second vibrational level leave the reaction path, in contrast with F + DBr($v = 2$). This discrepancy may be explained as follows: First, the skew angle ϕ_m between the educt and product potential valleys is smaller for F + MuBr than for F + DBr (cf. eq 2.5 and Figures 1 and 3). Second, the vibrational energies E_v of F + MuBr(v) are larger than those of F + DBr(v) (compare Figures 2 and 4). Both isotope effects of ϕ_m and E_v imply that corner cutting and hence the radial range of the dynamical white spot increase more efficiently with vibrational excitation of F + MuBr(v) than with excitation of F + DBr(v). Hence, criterion 2.15 is more easily satisfied for F + MuBr(v) than for F + DBr(v).

3.3. Reaction Dynamics on Modified Potential Energy Surfaces. The F + DBr($v = 0$) reaction dynamics on two adequate potential surfaces V_1 (eq 2.7) and V_2 (eq 2.8) are compared classically in parts a and d of Figure 1 and quantum mechanically in Figure 2 (see also Table II). Apparently the ground-state educts react along the reaction path ξ_1 of V_1 but not along ξ_2 of V_2. This remarkable discrepancy, induced by a small modification (eq 2.9) of the potentials, may be explained by a static plus a dynamical effect:

First, by construction, the reaction path ξ_2 penetrates farther into the potential corner than ξ_1; thus eq 3.1 applies (cf. eq 2.10) and Figure 1).

$$r_{min}(\xi_2) < r_{min}(\xi_1) \tag{3.1}$$

Second, the hyperspherical potential curves $\mathcal{E}_{v_3}(r)$ of V_2 are shifted to slightly larger energies than those of V_1 (see Figure 2) due to the small Gaussian shoulder (eq 2.9) of V_2 superimposed on V_1. Hence, by definition (eq 2.13), the radial boundaries $r_{v,qu}$ of the dynamical white spot of V_2 are also slightly larger than those of V_1 (see Figure 2). These shifts of quantum $r_{v,qu}$ also correspond to equivalent shifts of the boundaries to classical trajectories; compare, e.g., $r_{0,cl}$ for V_1 in Figure 1a with the larger $r_{0,cl}$ for V_2 in Figure 1d (see also Table II). In conclusion, all radial boundaries for educts F + DBr(v) reacting on V_1 or V_2 satisfy eq 3.2. Both the static effect (eq 3.1) and the dynamical effect

$$r_v(V_1) < r_v(V_2) \tag{3.2}$$

(eq 3.2) imply that criterion 2.15 is more easily fulfilled for V_2 than for V_1. In fact, the reaction path ξ_2 penetrates into the dynamical white spot of educts F + DBr($v = 0$) on potential V_2, in contrast with ξ_1.

4. Conclusions

The present investigations of the collinear F + DBr(v) and F + MuBr(v) reactions 2.1 and 2.2 on two potentials V_1 and V_2 (eq 2.7 and 2.8) demonstrate that chemical reactions do not necessarily react along the reaction path ξ, even at high energies well above the tunneling regime. The results imply the following conclusions:

(1) Strong deviations from the reaction path may be induced by vibrational excitation of educts. In extreme cases, depending on the system, the reaction may even avoid the potential barrier ‡, which by definition is the most integral part of ξ. This situation, which may appear paradoxical on traditional bias, has been demonstrated, e.g. in Figure 1c.

The resulting deviations from ξ are similar to tunneling paths avoiding the saddle point,[3,6-10] but the two mechanisms of vibrationally induced corner cutting at high energies and tunneling below the classical reaction threshold are entirely different, yielding opposite energetic trends: Deviations by tunneling decrease with translational energy of educts, in contrast with deviations due to vibrationally induced corner cutting, which increase with vibrational energy of educts. Moreover, both mechanisms are independent since the presence of one of them does not necessarily imply the other, for the same system. In the present case, F + DBr(v) exhibits vibrationally induced corner cutting but hardly any tunneling-induced corner cutting. In fact, analyses by S matrix propagation along r (see ref 15a) indicate that the F + DBr tunneling paths should not deviate significantly from the minimum energy reaction path ξ (see ref 15b), because the barrier is located rather early in the F + DBr educt valley where ξ is (almost) a straight line without curvature (see Figure 1c). It would be interesting to test this result by the least action (ground-state) variational methods.[9] Conversely, symmetric systems with barriers in the potential corner are good candidates for the simultaneous occurrence of tunneling-induced corner cutting (as demonstrated e.g. for Cl + HCl; see ref 9b,c and 19g) as well as vibrationally induced corner cutting (as implied by the potential curves shown in Figure 7 of ref 19g).

(2) Vibrational excitation of educts is not a necessary condition for deviations from ξ. Even ground-state educts may leave the reaction path ξ, provided it penetrates sufficiently far into the dynamical white spot located in the potential corner (see Figure 1d).

(3) Detours away from ξ are facilitated by decreasing the mass of the transferred atom. Extrapolating this isotope effect, one should expect that other exoergic hydrogen-transfer reactions will also leave their reaction paths. Exoergicity, or equivalently endoergicity of the back reaction, is favorable, since they imply large dynamical white spots[15] of the potential; however, even (near-) thermoneutral hydrogen-transfer reactions, e.g. O + HCl → OH + Cl or symmetric systems such as Cl + HCl ⇌ ClH + Cl or $CH_4 + {}^{\bullet}CH_3 \rightleftharpoons {}^{\bullet}CH_3 + CH_4$, may avoid the reaction path, if missing exoergicity is compensated by enhanced educt vibrational excitation.

The conclusions 1–3 also suggest the following inferences:

(4) If the reaction does not react along the intrinsic reaction path, then it is apparently disadvantageous to use ξ as reference for evaluations of the reaction dynamics. For example, consider again the F + DBr($v = 10$) reaction illustrated in Figure 1c: The properties of ξ and its surroundings, including the barrier ‡, are completely ineffectual due to vibrationally enhanced corner cutting. Obviously, the reaction dynamics do not depend on ξ, and any theory relating properties of ξ or ‡ to the F + DBr($v = 10$) rate coefficient etc. should be inadequate. In general, other reference paths may be more appropriate than ξ, as suggested previously in ref 2b. More recently, Ruf and Miller have advocated the use of novel, exclusively Cartesian reaction paths,[27] which should be adequate for many systems and much simpler to use than ξ.

(27) Ruf, B. A.; Miller, W. H., preprint 1987.

The present examples provide a rather general caveat: The literature is abundant with barriers and other properties of the reaction paths for many systems. This information is often important; however, in many cases it will not be sufficient to describe the chemical reaction. In fact, pure calculations of ξ and ‡ may be irrelevant. In any case, they should be complemented by evaluations of the reaction dynamics.

(5) On the other hand, reactions that do not follow ξ are also advantageous, since they explore different parts of the potential energy surface V, depending on educt excitation (compare parts a–c of Figure 1). In principle, this variability should allow us to determine all these regions of V by inversion techniques. For example, "transition state spectroscopy"[28] would not only yield information on potential barriers ‡ using thermal educts but also on the potential ridge using excited educts; likewise, very fast ground-state educts would yield information about the potential corner[15] and so on.

(6) The avoidance of the potential barrier ‡ by selective educt preparation implies (by time-reversed trajectories or wave packets) that collision complexes prepared close to ‡ yield specific energy release: They cannot decay into arbitrary but only into specific educt or product states. This conclusion corroborates a theorem of Ruf and Miller,[27] i.e. isomerization from ‡ along ξ will invariably end up along the molecular mode with lowest frequency (and of the same symmetry as ξ), typically a skeleton or backbone mode but hardly ever a localized R–H vibration.

The present conclusions are based on investigations of the simple collinear model reactions 2.1 and 2.2, which are at the disposal of available classical *and* quantum mechanical techniques. In the future, these studies should be extended to multidimensional systems, including atom plus diatom reactions with nonlinear barrier configurations and polyatomic reactions. Certainly it is a challenge to discover novel deviations from reaction paths in these systems. Most promising candidates include branching reactions where the branching region for classical trajectories or quantum wave packets is localized at a valley ridge inflection point before the bifurcation of ξ[3,29] and reactions of large molecules with high excitation of selective vibrational modes perpendicular to ξ.

Acknowledgment. We thank P. L. Gertitschke for helpful discussions of the FDBr tunneling path, documented in ref 15b, Professor K. Ruedenberg for suggesting that branching reactions may also deviate from the reaction path, and Professor W. H. Miller for sending us his preprint[28] prior to publication. B.H. also thanks the Studienstiftung des deutschen Volkes for a scholarship. Generous financial support by the Deutsche Forschungsgemeinschaft and the Fonds der Chemischen Industrie is gratefully acknowledged. The computations were carried out on the Siemens 7.860L Fujitsu computer of the Rechenzentrum der Universität Würzburg.

Registry No. F, 14762-94-8; HBr, 10035-10-6; D_2, 7782-39-0; muon, 12587-60-9.

(28) (a) Arrowsmith, P.; Bartoszek, F. E.; Bly, S. H. P.; Carrington, T., Jr.; Carters, P. E.; Polanyi, J. C. *J. Chem. Phys.* **1980**, *73*, 5895. (b) Hering, P.; Brooks, P. R.; Curl, R. F., Jr.; Judson, R. S.; Lowe, R. S. *Phys. Rev. Lett.* **1980**, *44*, 687. (c) Jouvet, C.; Soep, B. *Chem. Phys. Lett.* **1983**, *96*, 426. (d) Maguire, T. C.; Brooks, P. R.; Curl, R. F.; Spence, J. H.; Ulvick, S. J. *J. Chem. Phys.* **1986**, *85*, 844.

(29) (a) Valtazanos, P.; Ruedenberg, K. *Theor. Chim. Acta* **1986**, *69*, 281. (b) Kraus, W. A.; DePristo, A. E. *Theor. Chim. Acta* **1986**, *69*, 309. (c) Basilevsky, M. V. *Theor. Chim. Acta* **1987**, *72*, 63. (d) Ruedenberg, K., private communication, 1987.

The Coordination of Bare Fe^+ to Aliphatic Isonitriles Differs from that of Fe^+ and Nitriles†

Karsten Eller, Carlito B. Lebrilla, Thomas Drewello, and Helmut Schwarz*

Contribution from the Institut für Organische Chemie der Technischen Universität Berlin, Strasse des 17. Juni 135, D-1000 Berlin 12, Federal Republic of Germany. *Received August 24, 1987*

Abstract: Circumstantial evidence is presented which suggests that both *side-on* and *end-on* complexes are formed in the reactions of aliphatic, unbranched isonitriles RNC (R = C_2H_5–*n*-C_6H_{13}) with Fe^+ in the gas phase. Depending on the chain length of the alkyl groups, two distinct processes are observed for either complexes upon collisional activation. One corresponds to oxidative addition of CH/CC bonds in the vicinity of the functional group to eventually cleave the R–NC bond (R = alkyl). This reaction, which is not observed for isomeric RCN/Fe^+ complexes, dominates for R = C_2H_5–C_4H_9 and is caused by a *side-on* complexation of the RNC triple bond. For isonitriles with R = C_5H_{11} and C_6H_{13}, this process is still operative; the major reaction, however, corresponds to H_2 loss which is shown to involve functionalization of remote CH bonds, as has been demonstrated earlier for RCN/M^+ complexes (M = Fe, Co, Ni). The experimental data further suggest that the binding energy of *side-on* complexes is larger for RNC/Fe^+ than for RCN/Fe^+. Metal ion induced isomerization of the type RNC → RCN does not seem to occur in the gas phase.

The comparison of the behavior between nitriles (RCN) and isonitriles (RNC) and their role in synthetis[1a] is of fundamental interest in both organic and organometallic chemistry.[1] While the two types of molecules behave similarly in many respects, they differ in others as, for example, in the direction of the dipole moment and, as will be shown in this communication, in their reaction with bare transition metal ions in the gas phase. Recent work has provided evidence that metal ions M^+ (M = Fe,[2-4] Co,[3,4] and Ni[4]) coordinate in the gas phase through the lone-pair electrons of the nitrogen atom of the nitrile resulting in an *end-on* complexation.[5] By using mass spectrometric techniques this type of complexation is reflected in highly site-specific, collision-induced[6] dissociation processes of these complexes which show that

Scheme I

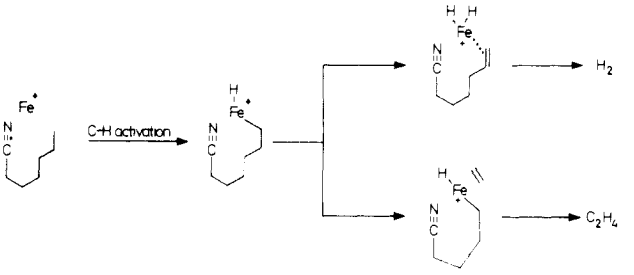

† Dedicated to Professor U. Schöllkopf, Göttingen, on the occasion of his 60th birthday.

0002-7863/88/1510-3068$01.50/0